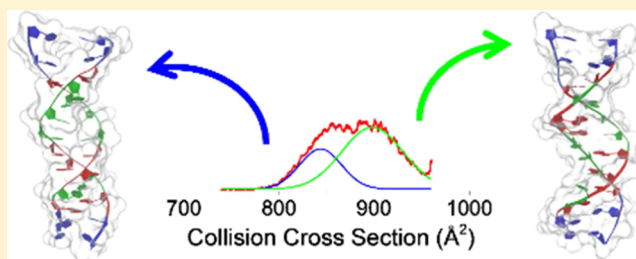


Differentiating Parallel and Antiparallel DNA Duplexes in the Gas Phase Using Trapped Ion Mobility Spectrometry

David Butcher,[†] Prem Chapagain,^{†,‡,§} Fenfei Leng,^{†,‡} and Francisco Fernandez-Lima^{*,†,‡,§}[†]Department of Chemistry & Biochemistry and [‡]Biomolecular Sciences Institute, Florida International University, Miami, Florida 33199, United States

Supporting Information

ABSTRACT: Deoxyribonucleic acids can form a wide variety of structural motifs which differ greatly from the typical antiparallel duplex stabilized by Watson–Crick base pairing. Many of these structures are thought to occur in vivo and may have essential roles in the biology of the cell. Among these is the parallel-stranded duplex—a structural motif in which DNA strands associate in a head-to-head fashion with the 5′ ends at the same end of the duplex—which is stabilized by reverse Watson–Crick base pairing. In this study, parallel- and antiparallel-stranded DNA duplexes formed from two different 12-mer oligonucleotides were studied using native electrospray ionization combined with trapped ion mobility spectrometry and mass spectrometry. The DNA duplex charge plays an important role in the gas-phase mobility profile, with a more compact form in negative mode than in positive mode ($\Delta\Omega \approx 100 \text{ \AA}^2$ between -4 and $+4$). Despite sequence mismatches, homo- and hetero-DNA duplexes were formed in solution and transfer to the gas phase, where a more compact structure was observed for the parallel compared to the antiparallel duplexes ($\Delta\Omega \approx 50 \text{ \AA}^2$), in good agreement with theoretical calculations. Theoretical studies suggest that a reduction (or compaction) along the helical axis of the parallel and antiparallel DNA duplexes is observed upon transfer to the gas phase.



INTRODUCTION

In vivo, DNA strands typically associate in an antiparallel fashion, forming a right-handed duplex with one strand running in the 5′ to 3′ direction, whereas the other strand runs in the 3′ to 5′ direction.¹ Adjacent purine and pyrimidine bases on each strand form Watson–Crick base pairs which stabilize the duplex. Genomic DNA that is not undergoing transcription exists largely in this conformation, either in the nucleoid in prokaryotes² or in the nucleus in eukaryotic cells where duplex DNA is complexed with histones.³ However, other tertiary and quaternary structural motifs can be formed depending on DNA sequence, solvent conditions, molecular crowding, and superhelical torsion. These structures include cruciforms,⁴ triplexes, G-quadruplexes,⁵ i-motifs,⁶ hairpins, and others. Many of these structural motifs have fundamental importance to biological processes in the cell, including transcription, replication, and DNA repair mechanisms,⁷ and dysfunction of these structural motifs and related protein binding partners is implicated in a wide variety of diseases. For example, the potential formation of the G-quadruplex and i-motif by guanine-rich and cytosine-rich sequences in human telomeres—which are often highly extended by overexpression of telomerase in cancerous cells⁸—and a large number of oncogenes⁹ has led to interest in these structures as drug targets.¹⁰

DNA sequences may also associate in a parallel fashion, resulting in a parallel duplex in which both strands run in the

same direction. The parallel-stranded duplex is stabilized by the formation of reverse Watson–Crick A–T or G–C base pairs.¹¹ Previous studies have established significant structural and spectroscopic differences between parallel- and antiparallel-stranded complexes.^{11,12} The formation of parallel-stranded duplexes has been observed in vitro in sequences from the genome of *Drosophila melanogaster*,¹³ suggesting that parallel-stranded duplexes, like other atypical DNA structural motifs, may be relevant in vivo.

The structure of DNA structural motifs in the gas phase has been characterized using molecular dynamics simulations and various ion mobility spectrometry techniques.^{14–17} It has been demonstrated that soft ionization techniques such as nano-electrospray ionization (nESI) can produce desolvated DNA molecular ions which retain a memory of their solution structure.¹⁵ In particular, we have demonstrated the analytical performance of nESI-TIMS-TOF MS technique for the characterization of i-motif DNA as a function of the solution conditions and intercalated cations.¹⁴

Here, native electrospray ionization combined with trapped ion mobility spectrometry (TIMS) and ultrahigh-resolution time-of-flight mass spectrometry (UHR-TOF-MS) was used for the first time to characterize the conformational space and

Received: December 20, 2017

Revised: May 29, 2018

Published: June 11, 2018

oligomerization states of two parallel strand-forming oligonucleotides: psDNA1 (5'-CCATAATTTACC-3') and psDNA2 (5'-CCTATTAAATCC-3'). These oligomers have been confirmed to form a parallel-stranded duplex in acidic solution through NMR spectroscopy.¹¹ The oligonucleotide sequences were chosen to minimize the formation of antiparallel duplexes and stabilize the parallel duplex at acidic pH by the formation of hemiprotonated cytosine base pairs¹¹ and to demonstrate that the separation of specific atypical DNA motifs is possible in the gas phase using TIMS. Other parallel-stranded duplex-forming oligonucleotides are possible but have not been reported in the literature. Hemiprotonated cytosine base pairs have also been observed under physiological pH conditions in the DNA i-motif because of an increase in pK_a of cytosine residues under molecular crowding conditions.¹⁸ Ion-neutral collision cross sections are reported for the psDNA1 and psDNA2 as a function of the charge state as well as their homo and heterodimer forms. Candidate structures are proposed to better understand the parallel and antiparallel duplex DNA structures.

METHODS AND MATERIALS

Preparation of Oligonucleotide Samples. DNA oligonucleotides with sequences 5'-CCATAATTTACC-3' (psDNA1) and 5'-CCTATTAAATCC-3' (psDNA2) were obtained in lyophilized form from Eurofins Genomics (Louisville, KY). Samples were prepared by dissolution of lyophilized oligonucleotides in type I ultrapure water for a final concentration of 100 μ M. For studies of the mixture of psDNA1 and psDNA2 oligonucleotides, 100 μ M stock solutions were mixed at a 1:1 ratio and allowed to anneal at 4 °C for at least 30 min before use to drive formation of DNA oligomers because very low formation of the dimeric species was observed at lower sample concentrations (\sim 10 μ M) at neutral pH. Analysis was performed at neutral pH (i.e., 10 mM ammonium acetate buffer) and by acidifying the solution (i.e., 1 v/v % Optima glacial acetic acid, Fisher Scientific) to enhance the dimer formation via hemiprotonated cytosine base pairing.

Native Polyacrylamide Gel Electrophoresis Analysis. Native polyacrylamide gel electrophoresis (PAGE) was used to visualize oligomers of psDNA1 and psDNA2. Samples were prepared by mixing oligonucleotides in ultrapure water with 6 \times loading dye containing Ficoll as well as xylene cyanol and bromophenol blue as tracking dyes. Oligonucleotides were run individually and as a mixture with \sim 2 μ g of total DNA loaded per lane. A 20% acrylamide gel was run at 180 V in a 4 °C cold room with 1 \times Trisacetate–ethylenediaminetetraacetic acid running buffer. SYBR Gold (Thermo Fisher) was used to stain the gel and bands were visualized in a UV lightbox (Figure S1).

TIMS—Mass Spectrometry Analysis. The operation of the TIMS cell (Figure S2) has been described elsewhere.^{19–21} The nitrogen bath gas flow is defined by the pressure differential between the entrance funnel ($P_1 = 2.6$ mbar) and the exit funnel ($P_2 = 1.1$ mbar) at ca. 293 K. A 880 kHz and 200 V_{pp} rf trapping potential was applied. Deflector, capillary, entrance funnel, entrance, and exit analyzer voltages were 60, 50, 0, –200 to 0, and 60 V, respectively, in positive mode (and –60, –50, 200–0, and –60 V in negative mode). These parameters have been optimized to prevent ion heating prior to IMS separation.²²

The mobility, K , of an ion in a TIMS cell is described by

$$K_0 = v_g/E \approx A/(V_{\text{elution}} - V_{\text{out}}) \quad (1)$$

where v_g , E , V_{elution} , and V_{out} are the gas velocity, applied electric field, elution voltage, and exit analyzer voltage, respectively. After thermalization, species were eluted from the TIMS cell by decreasing the electric field in stepwise decrements (referred to as the “ramp”) and can be described by a characteristic elution voltage (V_{elution}). Eluted ions were then mass-analyzed and detected by maXis impact Q-ToF MS (Bruker Daltonics Inc, Billerica, MA).

In a TIMS device, the total analysis time can be described as

$$\begin{aligned} \text{Total IMS time} &= t_{\text{trap}} + (V_{\text{elution}}/V_{\text{ramp}}) \times t_{\text{ramp}} + \text{TOF} \\ &= t_o + (V_{\text{elut}}/V_{\text{ramp}}) \times t_{\text{ramp}} \end{aligned} \quad (2)$$

where t_{trap} is the thermalization/trapping time, TOF is the time after the mobility separation, and V_{ramp} and t_{ramp} are the voltage range and time required to vary the electric field, respectively. The elution voltage was experimentally determined by varying the ramp time ($t_{\text{ramp}} = 100$ –500 ms) for a constant ramp voltage setting. The TIMS cell was operated using a fill/trap/ramp/wait sequence of 10/10/100–500/50 ms. The ToF analyzer was operated at 10 kHz (m/z 50–3500). The data were summed over 100 analysis cycles yielding an analysis time of \sim 50 s for the largest trapping times ($t_{\text{ramp}} = 500$ ms).

Mobility calibration was performed using the Tuning Mix calibration standard (G24221A, Agilent Technologies, Santa Clara, CA) in positive and negative ion mode (e.g., m/z 322, $K_0 = 1.376$ cm² V^{–1} s^{–1} and m/z 622, $K_0 = 1.013$ cm² V^{–1} s^{–1}).³² The TIMS operation was controlled using in-house software, written in National Instruments Lab VIEW, and synchronized with the maXis Impact Q-ToF acquisition program. A custom-built source using pulled capillary nESI emitters was utilized for all experiments. Quartz glass capillaries (O.D.: 1.0 mm and I.D.: 0.70 mm) were pulled utilizing a P-2000 micropipette laser puller (Sutter Instruments, Novato, CA) and loaded with \sim 10 μ L aliquot of the sample solution. A typical nESI source voltage of \pm 700–1500 V was applied between the pulled capillary tips and the TIMS-TOF MS instrument inlet. Ions were introduced via a stainless steel inlet capillary (1/16 \times 0.020”, IDEX Health Science, Oak Harbor, WA) held at room temperature into the TIMS cell.

Reduced mobility values (K_0) were correlated with collision cross section (Ω) using the Mason–Schamp equation

$$\Omega = \frac{(18\pi)^{1/2}}{16} \frac{z}{(k_B T)^{1/2}} \left[\frac{1}{m_i} + \frac{1}{m_b} \right]^{1/2} \frac{1}{K_0 N^*} \quad (3)$$

where z is the charge of the ion, k_B is the Boltzmann constant, N^* is the number density of the bath gas, and m_i and m_b refer to the masses of the ion and bath gas, respectively [33]. TIMS-MS spectra were analyzed using Compass Data Analysis 5.0 (Bruker Daltonik GmbH) and TIMS Data Viewer 1.4.0.31397 (Bruker Daltonik GmbH).

Theoretical Collision Cross Section Calculations. Initial guess structures for parallel-stranded psDNA1 and psDNA2 oligonucleotide heterodimers were taken from solution NMR studies of the parallel-stranded duplex (PDB ID 1JUJ).¹¹ In the case of the parallel-stranded psDNA1 and psDNA2 homodimers, the initial guess structures were taken from a parallel-stranded RNA duplex (PDB ID 5VXQ).²³ The initial guess structures for antiparallel-stranded psDNA1 and psDNA2 oligonucleotide homo and heterodimers were

generated in YASARA modeling software based on a B-DNA structure. All initial structures were subjected to annealing cycles followed by energy minimization using NAMD 2.12²⁴ and CHARMM36 forcefield.²⁵ Candidate structures were scaled (0.65 \times) along the helical axis for a better match to the experimental CCS distribution. This scaling factor is intended to compensate for deficiencies of molecular dynamics force fields in the description of base pairing and other interactions in the absence of the solvent, as suggested in previous mobility studies of DNA including the DNA i-motif.¹⁴ Theoretical CCS calculations were carried out in IMoS 1.06^{26,27} assuming the electrical charges at the center of mass of the molecule and using the elastic hard sphere scattering method.

RESULTS AND DISCUSSION

Analysis of psDNA1, psDNA2, and their mixture using native nESI-TIMS-TOF MS reveals the presence of molecular ions of oligonucleotide monomers with -2 , -3 , -4 , $+2$, and $+3$ charge states (Figures 1 and S2) in all three samples. Closer

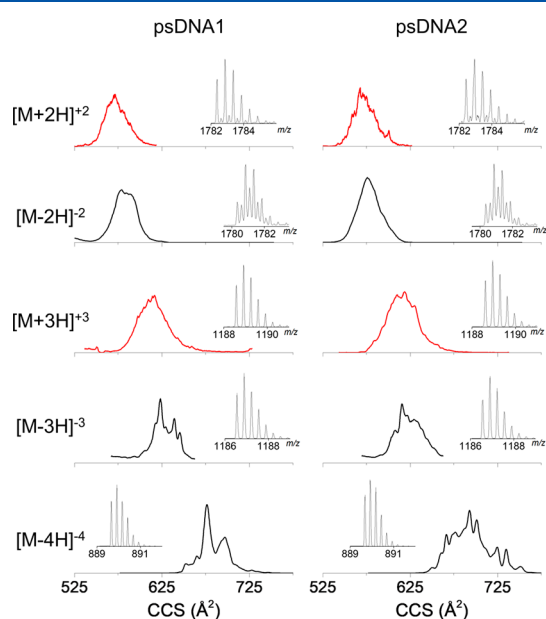


Figure 1. Mobility profiles for monomers formed by psDNA1 and psDNA2. Negative mode mobility profiles are shown in black and positive mode mobility profiles are shown in red. Mass spectra are shown as insets.

inspection of the mobility profiles of psDNA1 and psDNA2 monomers shows significant conformational heterogeneity (Figure 1). Although the lower charge state (-2 , $+2$, $+3$) mobility profiles appear as wide Ω distributions (e.g., 525–650 \AA^2) characteristic of an ensemble of conformations that cannot be independently resolved, the highest charge states (-3 and -4) show a more discrete profile with a large number of resolved features ($<10 \text{\AA}^2$ wide). We interpret these results as a consequence of the higher coulombic repulsion at higher charge states that translates into more elongated and less flexible conformational states that can be easily resolved due to the high resolution of the mobility analyzer.

Although the range of dimers that can be formed from the observed monomers is -4 to -8 and $+4$ to $+5$, only the lowest charge states (-4 , -5 , and $+4$) are observed (Figures 2 and S3). The observation of dimers for psDNA1, psDNA2, and

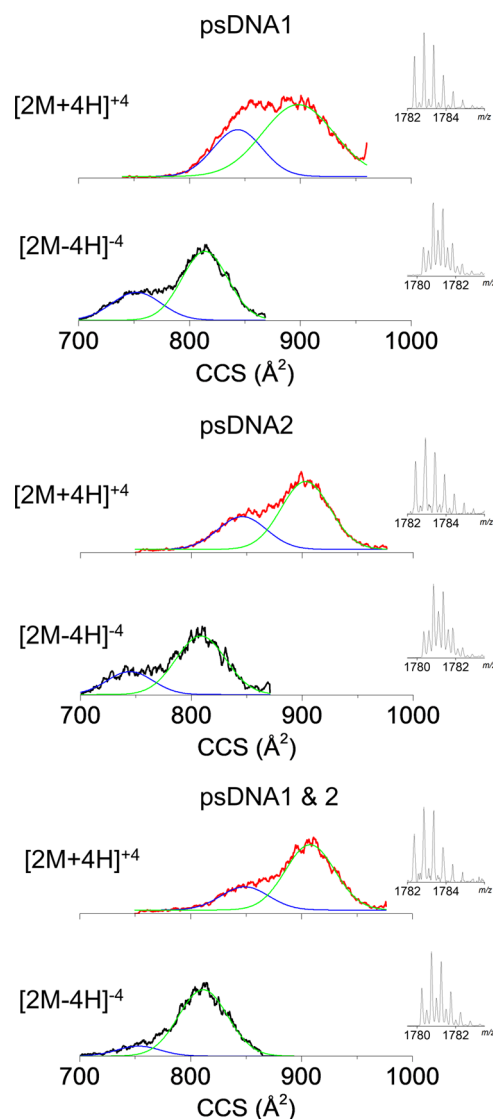


Figure 2. Mobility profiles for dimers formed by psDNA1 (top), psDNA2 (middle), and a mixture of both oligonucleotides (bottom). Gaussian fits to mobility profiles for parallel- and antiparallel-stranded conformations are shown in blue and green, respectively. Mass spectra are shown as insets.

their mixture using nESI-TIMS-TOF MS is consistent with solution experiments. For example, native PAGE analysis showed the presence of dimer bands for both oligonucleotides psDNA1 and psDNA2 and their mixture (Figure S1). Moreover, previous NMR studies also demonstrated the formation of psDNA1 and psDNA2 dimers in solution.¹¹ The narrow distribution of charge states observed in positive mode is consistent with that observed for the intramolecular i-motif, another DNA structural motif stabilized by hemiprotonated cytosine base pairs,¹⁴ and can be due to the decreased number of protonation sites available upon formation of the motif. Alternatively, nonspecific and highly charged dimers may more easily dissociate into monomers because of the lack of stabilizing intramolecular interaction and stronger coulombic repulsion at high charge states.

Closer inspection of the psDNA1 and 2 homo and heterodimer mobility profiles for the $+4/-4$ and -5 charge states showed two and one broad mobility bands ($\sim 100 \text{\AA}^2$) regardless of the starting solution composition (i.e., native vs

acidic solution), respectively (see details in Table 1). Although the pH does not affect the dimer mobility profiles, higher

Table 1. Experimental Ω Values for Mobility Bands Observed for +4 and -4 Dimers of psDNA1, psDNA2, and Their Mixture

sample	charge state	expt. collision cross section (\AA^2)	
		band 1	band 2
psDNA1	+4	843	898
	-4	752	814
psDNA2	+4	846	903
	-4	745	809
psDNA1 & psDNA2	+4	849	908
	-4	753	811

dimer intensity was observed at lower pH because the dimer formation is favored by hemiprotonation of the cytosines (see example of psDNA 1 +4 dimer mobility profile at native conditions in Figure S4). The mobility analysis did not show a dependence on the time after desolvation, indicating that the observed conformations of the dimers in the gas phase are stabilized quickly (<20 ms) and remain stable over the TIMS experiment (50–350 ms).

Possible duplex structures for the psDNA1 and 2 homo and heterodimers are shown in Figure 3 in the parallel and antiparallel form. That is, psDNA1 and psDNA2 oligonucleotides can form homo or heterodimers in which the strands are associated in a parallel or antiparallel fashion for a total of six unique configurations: two heterodimers and four homodimers. All dimers except the parallel heterodimer include mismatched bases as shown in Figure 3. The antiparallel heterodimer and antiparallel homodimers 1 and 2 have four mismatches, whereas parallel homodimers 1 and 2 have eight mismatches. Candidate structures were created following templates of previously reported parallel-stranded duplexes and following a B-DNA template for the antiparallel-stranded duplexes (see Figure 3 and Table 2). When compared to the experimental results, the theoretically predicted DNA duplexes require a compaction along the helical axis (scaling of 0.65) to match the gas-phase Ω . This DNA compaction is in good agreement with previous classical molecular dynamics simulations and mobility studies of oligomers of oligonucleotides^{14–17,28} and may be a consequence of the lack of accurate force field to treat charged nucleotide residues in the absence of a solvent. This differs from analogue studies using proteins, where a good agreement is typically observed between experimental and theoretical Ω from candidate structures determined by solution NMR, X-ray crystallography, or theoretical modeling.²⁹ It should be noted that these dimer candidate structures (Figure 3) do not describe the charge localization and intramolecular interactions that govern the true gas-phase structure of the duplex; there is a need of better force fields to better characterize the DNA intramolecular interactions, particularly when the base pairs are protonated. Molecular dynamics simulations have predicted that while the gross fold of the DNA helix is maintained, a significant number of base-pairing and stacking interactions are lost because of the distortion of the backbone structure.¹⁵ These constructs therefore only serve as “guiding” candidate structures for the purpose of assigning the observed mobility bands: parallel versus antiparallel.

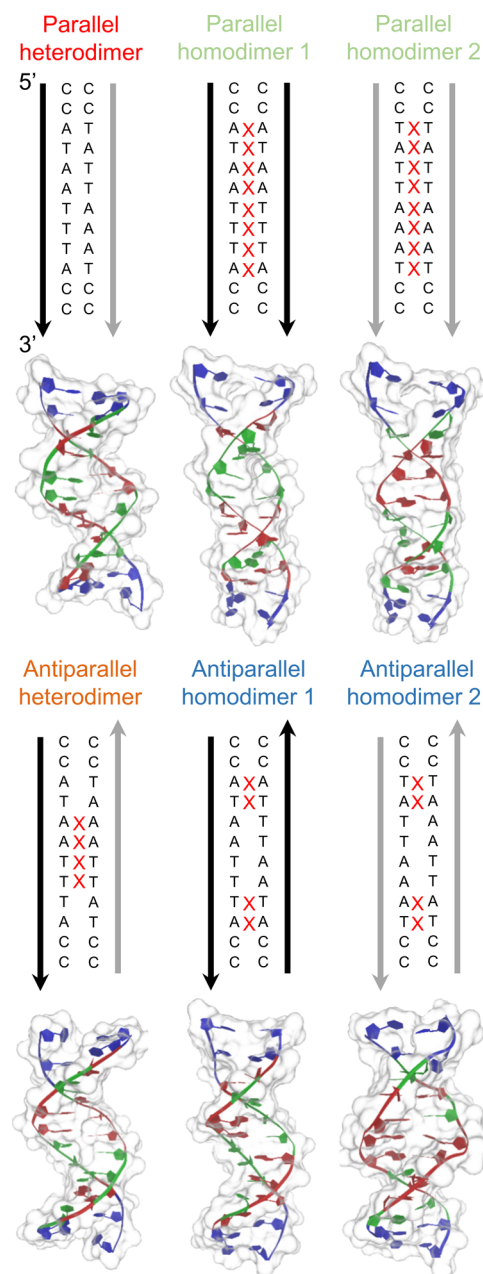


Figure 3. Scheme and candidate structures for psDNA1 and psDNA2 homo and hetero dimers in parallel and antiparallel configuration. Above, the phosphate–sugar backbones of psDNA1 and psDNA2 are shown as black and gray lines and base-pairing mismatches are denoted in red. Below, candidate structures are shown with cytosine, adenine, and thymine residues shown in blue, red and green respectively.

Inspection of the theoretical and experimental Ω for the psDNA1 and 2 homo and heterodimers suggests that the two mobility bands correspond to a parallel and antiparallel construct. For example, theoretical Ω values for the +4 parallel and antiparallel heterodimers match well with the values for each of the observed mobility bands—845 versus 846 \AA^2 and 894 versus 903 \AA^2 , respectively. That is, the lower Ω band in the mixture of psDNA1 and 2 corresponds to the parallel heterodimer, whereas the larger Ω band corresponds to the antiparallel heterodimer. The trend of the theoretical Ω for the antiparallel-stranded dimer being larger than that for the

Table 2. Theoretical Ω Calculated for the Proposed Candidate Structures of the psDNA1/psDNA2 Dimer Constructs

structure	charge state	theoretical collision cross section (\AA^2)
parallel heterodimer	+4	845
	-4	847
parallel homodimer 1	+4	863
	-4	879
parallel homodimer 2	+4	852
	-4	892
antiparallel heterodimer	+4	895
	-4	922
antiparallel homodimer 1	+4	886
	-4	935
antiparallel homodimer 2	+4	865
	-4	889

parallel-stranded dimer holds true for most of the +4/-4 constructs. Nearly identical Ω values are measured for the two bands in the mobility profiles of psDNA1 and psDNA2 individually as compared to the mixture; therefore, we assign the lower Ω bands to the parallel homodimers and the higher Ω bands to the antiparallel homodimers. The mobility bands for the mixture of psDNA1 and psDNA2 most likely correspond to a mixture of both heterodimers and homodimers formed by the individual oligonucleotides; however, we are unable to determine the ratio of homo to heterodimers in the mixture because of their very similar mobilities.

A common trend in the +4/-4 dimer IMS profiles is the larger Ω values observed in positive with respect to negative mode. The backbone phosphates and cytosine bases have the highest and second highest gas-phase basicity values of the moieties found in the oligonucleotide,³⁰ so in negative mode, protons are likely to be abstracted from the protonated cytosine bases which participate in hemiprotonated cytosine base pairs. The disruption of these interactions could lead to structural changes which result in a more compact Ω (notice that this is not considered in the theoretical workflow utilized here). Therefore, in positive mode (+4), the DNA can maintain a pattern of protonation closer to that in solution, where the cytosine bases are largely protonated and able to form hemiprotonated cytosine base pairs. This hypothesis is also consistent with the larger Ω observed for the -5 relative to the -4 dimers (see Figure S3); a charge-driven structural transition occurs from -4 to -5 dimers leading to more unfolded structures.

It is interesting that we see the formation of parallel homodimers of psDNA1 and psDNA2, which have eight base-pair mismatches. Mass spectrometry³¹ and spectroscopic and calorimetric studies³² of DNA duplexes have shown that a single mismatch can destabilize the duplex and that AA and TT mismatches are among the most energetically unfavorable. Nonetheless, the observation of parallel homodimers in our mobility profiles and native PAGE experiments shows that these structures are formed in solution and are maintained in the gas phase. The formation of hemiprotonated cytosine base pairs at the ends of the duplexes may help to stabilize these duplexes in solution despite the unfavorability of the AA and TT mismatches. This observation also supports the idea that other nonspecific duplexes can be formed in solution, in good

agreement with the wide mobility bands observed for the homo and heterodimers.

In addition to examining the Ω values, we can compare the relative abundance of the parallel and antiparallel duplexes by comparison of the mobility band intensities. For the +4 dimers, the ratio of antiparallel-to-parallel duplex mobility band intensity for psDNA1 is approximately 1.5:1 and increases to 2.1:1 for psDNA2 and 2.6:1 for the mixture of both oligonucleotides. For the -4 dimers, the ratio of antiparallel-to-parallel intensities is about 2.6:1 for psDNA1 and psDNA2 and increases greatly to about 7:1 for the mixture. In the gas phase, relative intensities of the mobility bands reflect the relative abundances of the antiparallel and parallel duplexes and their abundances in solution prior to ionization/desolvation, which is a function of the energetics of formation of each dimer, that is, dimers whose formation is more energetically favorable will tend to predominate in solution. From this, we conclude that for the +4 and -4 charge states, the formation of the antiparallel homo and heterodimer is overall more favorable than that of parallel homo and heterodimer. The increased ratio of antiparallel to parallel for the -4 dimers may be due to abstraction of protons during the ionization process. Deprotonation of cytosine residues involved in hemiprotonated base pairs could destabilize the parallel duplex, causing it to dissociate into monomers in the gas phase. This effect is particularly pronounced for the -4 dimers of the mixture of psDNA1 and psDNA2, where the intensity of the mobility band for the parallel hetero and homodimers (which have the same Ω) is only about 1/7th of that for the antiparallel hetero and homodimers.

CONCLUSIONS

In this study, we have demonstrated for the first time that a parallel-stranded (noncanonical reverse Watson-Crick base pairing) and an antiparallel-stranded (Watson-Crick base pairing) DNA structure can be studied in the gas phase using TIMS-MS. Homo and heterodimers of parallel- and antiparallel-stranded structures were separated based on their differences in Ω , demonstrating the benefit of ion mobility-mass spectrometry for the study of DNA structures.

Mobility profiles for the monomers of psDNA1 and psDNA2 display a large number of individual conformations, showing that DNA monomers have great structural heterogeneity in the gas phase. We see two mobility bands for the +4 and -4 dimers formed by psDNA1, psDNA2, and in the mixture, indicating that there are two major conformations of the duplex in the gas phase. Complementary theoretical studies allow us to assign the bands at ~ 850 and 900 \AA^2 to the parallel- and antiparallel-stranded structures, respectively.

We have shown that DNA structures undergo compaction upon transfer to the gas phase, resulting in observed Ω values significantly smaller than theoretical predictions based on solution-phase structures. There is also a significant difference in Ω for parallel- and antiparallel-stranded duplexes measured in positive mode and negative mode. Changes in the pattern of protonation as a result of the ionization process are likely responsible for the significantly smaller Ω values observed in negative mode as compared to positive mode ($\Delta\Omega \approx 100 \text{ \AA}^2$). In positive mode, DNA monomers and dimers can maintain a pattern of protonation similar to that in the solution phase. On the other hand, protons must be abstracted from the protonated backbone phosphates and nucleic acid bases in negative mode, leading to structural changes in the gas phase

which result in a more compact conformation and smaller Ω . We also observe a greater abundance of the antiparallel-stranded conformations compared to parallel-stranded conformations despite the mismatches present (by design) in all possible antiparallel duplexes, indicating that the hemiprotonated cytosine base pairs formed by the cytosine residues at the 5' and 3' ends of each oligonucleotide provide a strong stabilizing interaction which can overcome the energetic unfavorability of the AA and TT mismatches.

■ ASSOCIATED CONTENT

■ Supporting Information

The Supporting Information is available free of charge on the ACS Publications website at DOI: 10.1021/acs.jpcc.7b12544.

Native PAGE, Schematic of the TIMS cell, combined mass spectra and mobility profiles for monomers and dimers of all charge states, and separate mobility profiles for -5 dimers (PDF)

■ AUTHOR INFORMATION

Corresponding Author

*E-mail: fernandf@fiu.edu.

ORCID

Prem Chapagain: 0000-0002-0999-4975

Francisco Fernandez-Lima: 0000-0002-1283-4390

Notes

The authors declare no competing financial interest.

■ ACKNOWLEDGMENTS

This work was supported by the National Science Foundation Division of Chemistry, under CAREER award CHE-1654274, with cofunding from the Division of Molecular and Cellular Biosciences to F.F.-L. The authors would also like to acknowledge the helpful discussions and technical support from Dr. Mark E. Ridgeway and Dr. Melvin A. Park from Bruker Daltonics Inc. during the development and installation of the custom-built TIMS-TOF MS instrument.

■ REFERENCES

- (1) Watson, J. D.; Crick, F. H. C. Molecular Structure of Nucleic Acids: A Structure for Deoxyribose Nucleic Acid. *Nature* **1953**, *171*, 737–738.
- (2) Thanbichler, M.; Wang, S. C.; Shapiro, L. The Bacterial Nucleoid: A Highly Organized and Dynamic Structure. *J. Cell. Biochem.* **2005**, *96*, 506–521.
- (3) Kornberg, R. D. Chromatin Structure: A Repeating Unit of Histones and DNA. *Science* **1974**, *184*, 868–871.
- (4) Bra'zda, V.; Laister, R. C.; Jagelska', E. B.; Arrowsmith, C. Cruciform Structures are a Common DNA Feature Important for Regulating Biological processes. *BMC Mol. Biol.* **2011**, *12*, 33.
- (5) Sen, D.; Gilbert, W. Formation of Parallel Four-stranded Complexes by Guanine-rich Motifs in DNA and its Implications for Meiosis. *Nature* **1988**, *334*, 364–366.
- (6) Guéron, M.; Leroy, J.-L. The I-motif in Nucleic Acids. *Curr. Opin. Struct. Biol.* **2000**, *10*, 326–331.
- (7) Zhao, J.; Bacolla, A.; Wang, G.; Vasquez, K. M. Non-B DNA Structure-induced Genetic Instability and Evolution. *Cell. Mol. Life Sci.* **2010**, *67*, 43–62.
- (8) Campbell, P. J. Telomeres and Cancer: From Crisis to Stability to Crisis to Stability. *Cell* **2012**, *148*, 633–635.
- (9) Brooks, T. A.; Kendrick, S.; Hurley, L. Making Sense of G-quadruplex and I-motif Functions in Oncogene Promoters. *FEBS J.* **2010**, *277*, 3459–3469.
- (10) Sun, D.; Hurley, L. H. The Importance of Negative Superhelicity in Inducing the Formation of G-Quadruplex and i-Motif Structures in the c-Myc Promoter: Implications for Drug Targeting and Control of Gene Expression. *J. Med. Chem.* **2009**, *52*, 2863–2874.
- (11) Parvathy, V. R.; Bhaumik, S. R.; Chary, K. V. R.; Govil, G.; Liu, K.; Howard, F. B.; Miles, H. T. NMR Structure of a Parallel-stranded DNA Duplex at Atomic Resolution. *Nucleic Acids Res.* **2002**, *30*, 1500–1511.
- (12) Vorlíčkova', M.; Kejnovska', I.; Bedna'řova', K.; Renčíuk, D.; Kypr, J. Circular Dichroism Spectroscopy of DNA: From Duplexes to Quadruplexes. *Chirality* **2012**, *24*, 691–698.
- (13) Tchurikov, N. A.; Chernov, B. K.; Golova, Y. B.; Nechipurenko, Y. D. Parallel DNA: Generation of a Duplex between Two Drosophila Sequences In Vitro. *FEBS Lett.* **1989**, *257*, 415–418.
- (14) Garabedian, A.; Butcher, D.; Lippens, J. L.; Miksovská, J.; Chapagain, P. P.; Fabris, D.; Ridgeway, M. E.; Park, M. A.; Fernandez-Lima, F. Structures of the Kinetically Trapped I-motif DNA Intermediates. *Phys. Chem. Chem. Phys.* **2016**, *18*, 26691–26702.
- (15) Abi-Ghanem, J.; Gabelica, V. Nucleic Acid Ion Structures in the Gas Phase. *Phys. Chem. Chem. Phys.* **2014**, *16*, 21204–21218.
- (16) Arcella, A.; Portella, G.; Ruiz, M. L.; Eritja, R.; Vilaseca, M.; Gabelica, V.; Orozco, M. Structure of Triplex DNA in the Gas Phase. *J. Am. Chem. Soc.* **2012**, *134*, 6596–6606.
- (17) Gidden, J.; Baker, E. S.; Ferzoco, A.; Bowers, M. T. Structural Motifs of DNA Complexes in the Gas Phase. *Int. J. Mass Spectrom.* **2005**, *240*, 183–193.
- (18) Rajendran, A.; Nakano, S.-i.; Sugimoto, N. Molecular Crowding of the Cosolutes Induces an Intramolecular I-motif Structure of Triplet Repeat DNA Oligomers at Neutral pH. *Chem. Commun.* **2010**, *46*, 1299–1301.
- (19) Fernandez-Lima, F.; Kaplan, D. A.; Suetering, J.; Park, M. A. Gas-phase Separation Using a Trapped Ion Mobility Spectrometer. *Int. J. Ion Mobility Spectrom.* **2011**, *14*, 93–98.
- (20) Fernandez-Lima, F. Trapped Ion Mobility Spectrometry: Past, Present and Future Trends. *Int. J. Ion Mobility Spectrom.* **2016**, *19*, 65–67.
- (21) Hernandez, D. R.; DeBord, J. D.; Ridgeway, M. E.; Kaplan, D. A.; Park, M. A.; Fernandez-Lima, F. Ion Dynamics in a Trapped Ion Mobility Spectrometer. *Analyst* **2014**, *139*, 1913–1921.
- (22) Liu, F. C.; Kirk, S. R.; Bleiholder, C. On the Structural Denaturation of Biological Analytes in Trapped Ion Mobility Spectrometry - Mass Spectrometry. *Analyst* **2016**, *141*, 3722–3730.
- (23) Copp, W.; Denisov, A. Y.; Xie, J.; Noronha, A. M.; Liczner, C.; Safaee, N.; Wilds, C. J.; Gehring, K. Influence of Nucleotide Modifications at the C2' Position on the Hoogsteen Base-paired Parallel-stranded Duplex of Poly(A) RNA. *Nucleic Acids Res.* **2017**, *45*, 10321–10331.
- (24) Phillips, J. C.; Braun, R.; Wang, W.; Gumbart, J.; Tajkhorshid, E.; Villa, E.; Chipot, C.; Skeel, R. D.; Kalé, L.; Schulten, K. Scalable Molecular Dynamics with NAMD. *J. Comput. Chem.* **2005**, *26*, 1781–1802.
- (25) Brooks, B. R.; Bruccoleri, R. E.; Olafson, B. D.; States, D. J.; Swaminathan, S.; Karplus, M. CHARMM: A Program for Macromolecular Energy, Minimization, and Dynamics Calculations. *J. Comput. Chem.* **1983**, *4*, 187–217.
- (26) Larriba, C.; Hogan, C. J. Free Molecular Collision Cross Section Calculation Methods for Nanoparticles and Complex Ions with Energy Accommodation. *J. Comput. Phys.* **2013**, *251*, 344–363.
- (27) Larriba, C.; Hogan, C. J. Ion Mobilities in Diatomic Gases: Measurement versus Prediction with Non-Specular Scattering Models. *J. Phys. Chem. A* **2013**, *117*, 3887–3901.
- (28) Rueda, M.; Kalko, S. G.; Luque, F. J.; Orozco, M. The Structure and Dynamics of DNA in the Gas Phase. *J. Am. Chem. Soc.* **2003**, *125*, 8007–8014.
- (29) Molano-Arevalo, J. C.; Fouque, K. J. D.; Pham, K.; Miksovská, J.; Ridgeway, M. E.; Park, M. A.; Fernandez-Lima, F. Characterization of Intramolecular Interactions of Cytochrome c Using Hydrogen-Deuterium Exchange-Trapped Ion Mobility Spectrometry—Mass

Spectrometry and Molecular Dynamics. *Anal. Chem.* **2017**, *89*, 8757–8765.

(30) Moser, A.; Range, K.; York, D. M. Accurate Proton Affinity and Gas-Phase Basicity Values for Molecules Important in Biocatalysis. *J. Phys. Chem. B* **2010**, *114*, 13911–13921.

(31) Pan, S.; Sun, X.; Lee, J. K. Stability of Complementary and Mismatched DNA Duplexes: Comparison and Contrast in Gas versus Solution Phases. *Int. J. Mass Spectrom.* **2006**, *253*, 238–248.

(32) Tikhomirova, A.; Beletskaya, I. V.; Chalikian, T. V. Stability of DNA Duplexes Containing GG, CC, AA, and TT Mismatches. *Biochemistry* **2006**, *45*, 10563–10571.